DALTON
FULL PAPER

Formation of organically surface-modified metal oxo clusters from carboxylic acids and metal alkoxides: a mechanistic study

Guido Kickelbick,*[a] Martin P. Feth,[b] Helmut Bertagnolli,[b] Michael Puchberger,[a] Dieter Holzinger[a] and Silvia Gross[a]

[a] *Institut für Materialchemie, Technische Universität Wien, Getreidemarkt 9/165, A-1060 Wien, Austria. E-mail: guido.kickelbick@tuwien.ac.at*
[b] *Institut für Physikalische Chemie, Universität Stuttgart, Pfaffenwaldring 55, D-70550 Stuttgart, Germany*

Received 14th August 2002, Accepted 23rd August 2002
First published as an Advance Article on the web 16th September 2002

The reaction of $Zr(OR)_4$ (OR = O^nBu, O^nPr) with methacrylic acid was monitored by extended X-ray absorption fine structure (EXAFS), ^1H and ^{13}C NMR, HPLC, and Raman measurements. The study revealed that the initial dimeric zirconium alkoxides react rapidly with the carboxylic acid and form higher aggregated multinuclear compounds. EXAFS investigations showed that the structures of the resulting aggregates in solution depend on the carboxylic acid to alkoxide ratio. In addition, the reaction rates also differ depending on this ratio; while for a methacrylic acid to zirconium alkoxide ratio of 4:1 the reaction is slow, metal oxo clusters form rapidly with a 7:1 ratio. Methacrylic acid ester is simultaneously formed during the reaction, with concomitant production of water, required for the formation and condensation reactions in the cluster preparation.

Introduction

In recent years, the formation of inorganic–organic hybrid materials, in particular nanocomposites, has attracted a great deal of interest.[1–4] For the formation of these materials, the sol–gel process is often used due to its mild solvent-based conditions. Contrary to the easily controllable conditions of the silicon-based sol–gel process, transition metal alkoxides require a reduction of their reactivity to avoid immediate precipitation of the metal oxide after water addition.[1] For this purpose, carboxylic acids that coordinate to the metal as bidentate ligands, and thus reduce the reactivity of the precursor, are added. Furthermore, the addition of carboxylic acids to metal alkoxides may also produce *in situ* well-defined surface-modified crystalline metal oxo clusters of the general formula $M_wO_x(OR)_y(OOC–FG)_z$ (FG = functional group). A plethora of different clusters of this type have already been discovered and characterized. The composition and the structures depend on the metal alkoxide, the carboxylic acid, and the ratio between them.[5–11] A three-step mechanism was proposed for the formation of the clusters (Scheme 1): (i) the partial substitution

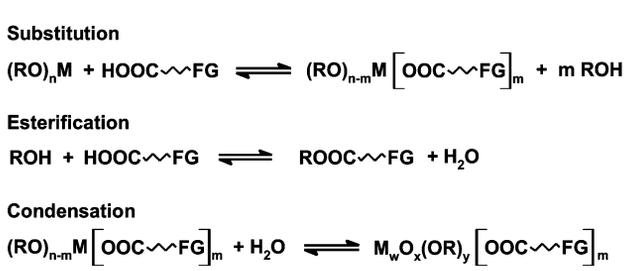

Scheme 1

of alkoxide groups at the metal by carboxylic acids; (ii) the formation of an ester by the reaction of free carboxylic acid and the released alcohol, and, hence, the controlled production of water; (iii) the condensation of partially substituted building blocks in solution. Furthermore, a related four-step mechanism based on a comprehensive study of the reaction between titanium alkoxides and acetic acid was proposed to be general for the mixture of carboxylic acids and metal alkoxides.[5] The confirmation of this proposed reaction scheme by a single analytical technique is difficult because conventional spectroscopic methods do not allow a reliable insight into the reactions that take place in the solution. Hence, to prove the reaction mechanism and to get information on the rate of cluster formation in solution, a variety of different analytical methods has to be applied simultaneously. This paper presents the data obtained by HPLC, EXAFS, Raman, and NMR spectroscopy, and a comparison of the results with the data for well-defined reference compounds.

Results and discussion

EXAFS results

EXAFS spectroscopy provides structural information on the local environment of an X-ray absorbing atom. In particular, compounds containing metal atoms with high energy absorption edges (like Zr) are well suited for this method, while other atoms, like C, O, N, or halogens, do not contribute much to the total absorption. Hence, this method is ideal for the zirconium compounds investigated in the present study. An additional advantage compared to other X-ray techniques is that no crystalline material is required and even measurements in solutions are possible.[12] In a recent paper, we demonstrated that this method is suitable for the identification of surface-modified metal oxo clusters of Ti and Zr in organic polymer nanocomposites prepared from them.[13] For the present study, solutions of methacrylic acid (MAA) and $Zr(O^nBu)_4$, in typical ratios for cluster synthesis, were investigated and compared with the pure metal alkoxide and the final crystalline products to gain information about the evolution of the structural environment around the zirconium atoms in solution.

The $Zr_6(OH)_4O_4(OMc)_{12}$ (OMc = methacrylate ligand) cluster [Zr_6, Fig. 1(a)] crystallizes quantitatively from a mixture

 DOI: 10.1039/b207994a

Table 1 Structural parameters of the crystalline $Zr_6(OH)_4O_4(OMc)_{12}$ cluster, crystalline $Zr_4O_2(OMc)_{12}$, and pure zirconium n-butoxide, determined from the Zr *K*-edge EXAFS spectrum. The coordination numbers were fixed according to the averaged crystallographic values and to values known from the literature

	A–Bs	r^a/Å	N^b	σ^c/Å	$\Delta E_0{}^d$/eV	*k*-Range/Å^{-1}, fit index
$Zr(O^nBu)_4$	Zr–O	1.97 ± 0.02	2	0.053 ± 0.010	16.6	3.40–17.00, 37.2
	Zr–O	2.16 ± 0.02	2	0.050 ± 0.010		
	Zr–O	2.27 ± 0.02	2	0.072 ± 0.010		
	Zr–C	3.07 ± 0.03	2	0.084 ± 0.010		
	Zr–Zr	3.49 ± 0.04	1	0.076 ± 0.010		
$Zr(O^nBu)_4$ EXAFS[14]	Zr–O	1.96	1.7	0.032	18.2	3.00–13.00, 40.0
	Zr–O	2.12	1.9	0.022		
	Zr–O	2.27	1.9	0.045		
	Zr–C	3.09	1.5	0.059		
	Zr–Zr	3.52	1.0	0.074		
$Zr_6O_4(OH)_4(OMc)_{12}$ crystalline	Zr–O	2.10 ± 0.02	2	0.065 ± 0.007	20.6	3.51–16.00, 27.5
	Zr–O	2.24 ± 0.03	6	0.084 ± 0.013		
	Zr–Zr	3.51 ± 0.04	4	0.075 ± 0.022		
$Zr_6O_4(OH)_4(OMc)_{12}$ single crystal study[7]	Zr–O	2.07	2			
	Zr–O	2.21	6			
	Zr–Zr	3.51	4			
$Zr_4O_2(OMc)_{12}$ crystalline	Zr–O	2.20 ± 0.02	7.5	0.101 ± 0.010	18.8	3.51–16.00, 31.7
	Zr–Zr	3.32 ± 0.03	0.5	0.063 ± 0.013		
	Zr–Zr	3.51 ± 0.04	2	0.068 ± 0.020		
$Zr_4O_2(OMc)_{12}$ single crystal study[7]	Zr–O	2.07	7.5			
	Zr–Zr	3.30	0.5			
	Zr–Zr	3.67	2			

[a] Absorber (A)–backscatterer (Bs) distance. [b] Coordination number. [c] Debye–Waller factor, with its calculated deviation. [d] Energy threshold shift.

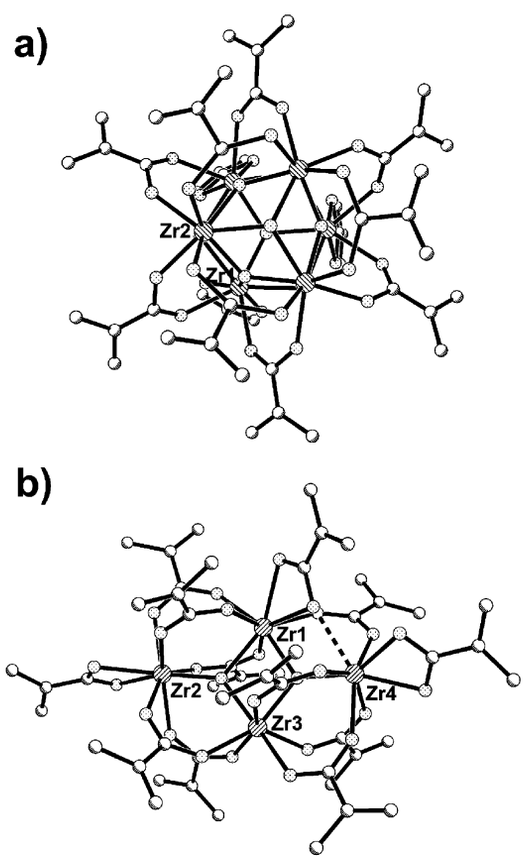

Fig. 1 Molecular structures of the clusters $Zr_6(OH)_4O_4(OMc)_{12}$ (a) and $Zr_4O_2(OMc)_{12}$ (b), as determined from single crystal X-ray data.[7]

of 80 wt% $Zr(O^nBu)_4$ in n-butanol and 4 molar equivalents of MAA after a few days. In the EXAFS investigation, an 80 wt% n-butanol solution of $Zr(O^nBu)_4$ was first measured as a standard, and then MAA was added. The data for the precursor $Zr(O^nBu)_4$ in n-butanol were in agreement with the results of a previous EXAFS analysis on metal alkoxides in solution (Table 1).[14] The zirconium atoms have three clearly distinguishable oxygen shells, with mean Zr–O distances of 1.97 (coordination number N = 2), 2.16 (N = 2), and 2.27 Å (N = 2). Two of these oxygen atoms stem from coordinated n-butanol. The Zr backscatterer (N = 1) at 3.49 Å proves that $Zr(O^nBu)_4$ has a dimeric structure in solution. The data in solution are consistent with the structural data obtained from single crystal X-ray analyses of pure and substituted zirconium alkoxides.[15–17] 60 min after the addition of four equivalents of methacrylic acid, the coordination number of the Zr backscatterer is increased to 1.5, and the mean Zr–Zr distance contracted to 3.42 Å (Table 2, Fig. 2). The three oxygen shells collapsed to one with a coordination number of 6.7 and a mean Zr–O distance of 2.22 Å. Additional measurements were carried out after several time intervals up to 1440 min using the same reaction solution. The data obtained by these measurements support the fast reaction rates between $Zr(O^nBu)_4$ and MAA. During the reaction, the average Zr–O distances remained at 2.20 Å and the coordination number of the oxygen atoms continuously increased up to a value of 7.4 ± 0.7. Both values are, within the standard deviations, similar to those of the crystalline $Zr_6(OH)_4O_4(OMc)_{12}$ cluster. This cluster, however, shows two distinguishable oxygen shells, whereas the reaction solution has only one shell with a mean Zr–O distance. The Zr–Zr distance of about 3.40 Å is shorter compared to the corresponding value in the crystalline cluster (3.51 Å), and also the Zr coordination number, which is 4 in the resulting cluster, is much lower, *viz.* 1.7 ± 0.3. A possible explanation is the formation of smaller fragments that already have the oxygen coordination of the resulting cluster around the zirconium, but are not condensed to the final octahedral Zr core of the cluster. Bridged trinuclear Zr species, which contain μ_3-O or μ_3-OR groups capping the face of a Zr_3 triangle (Zr coordination number = 2), are potential intermediates in the cluster formation (Scheme 2). Oxoalkoxides with this structural motif were already characterized by single crystal X-ray crystallography and show Zr–Zr distances of 3.22 Å.[18,19] A partly carboxylate-substituted trinuclear Zr compound is also known, in which longer (3.86 Å) and shorter Zr–Zr distances (3.37, 3.41 Å) were observed, depending on the bridging ligands.[20] Additionally, a cluster with the $Zr_3(\mu_3\text{-O})$ unit was the product of a reaction of $Zr(OPr)_4$ with 2,4-dimethylpentane-2,4-diol. The resulting compound showed Zr–Zr distances of around 3.40 Å.[21] Condensation of two such trinuclear units could lead to the octahedral cluster.

Table 2 Time-dependent structural parameters of a mixture of MAA and 80 wt% $Zr(O^nBu)_4$ in n-butanol (molar ratio: 4:1), determined from the Zr *K*-edge EXAFS spectrum

t/min	A–Bs	r^a/Å	N^b	σ^c/Å	$\Delta E_0{}^d$/eV	*k*-Range/Å^{-1}, fit index
60	Zr–O	2.22 ± 0.02	6.7 ± 0.7	0.098 ± 0.010	17.4	3.21–13.79, 25.6
	Zr–Zr	3.42 ± 0.03	1.5 ± 0.3	0.088 ± 0.017		
90	Zr–O	2.21 ± 0.02	6.7 ± 0.7	0.097 ± 0.010	18.2	3.21–13.79, 28.8
	Zr–Zr	3.42 ± 0.03	1.9 ± 0.4	0.092 ± 0.018		
120	Zr–O	2.21 ± 0.02	6.9 ± 0.7	0.099 ± 0.010	18.2	3.21–13.79, 30.2
	Zr–Zr	3.42 ± 0.03	1.9 ± 0.4	0.089 ± 0.018		
180	Zr–O	2.21 ± 0.02	6.8 ± 0.7	0.097 ± 0.010	17.9	3.21–13.79, 24.9
	Zr–Zr	3.42 ± 0.03	1.6 ± 0.4	0.081 ± 0.016		
360	Zr–O	2.21 ± 0.02	6.9 ± 0.7	0.098 ± 0.010	18.0	3.21–13.79, 25.5
	Zr–Zr	3.42 ± 0.03	1.7 ± 0.4	0.084 ± 0.018		
720	Zr–O	2.19 ± 0.02	7.5 ± 0.7	0.102 ± 0.010	18.9	3.22–12.00, 27.2
	Zr–Zr	3.40 ± 0.03	1.6 ± 0.4	0.081 ± 0.018		
1440	Zr–O	2.20 ± 0.02	7.4 ± 0.7	0.102 ± 0.010	18.8	3.27–14.00, 25.4
	Zr–Zr	3.40 ± 0.03	1.6 ± 0.3	0.082 ± 0.016		

[a] Absorber (A)–backscatterer (Bs) distance. [b] Coordination number. [c] Debye–Waller factor, with its calculated deviation. [d] Energy threshold shift.

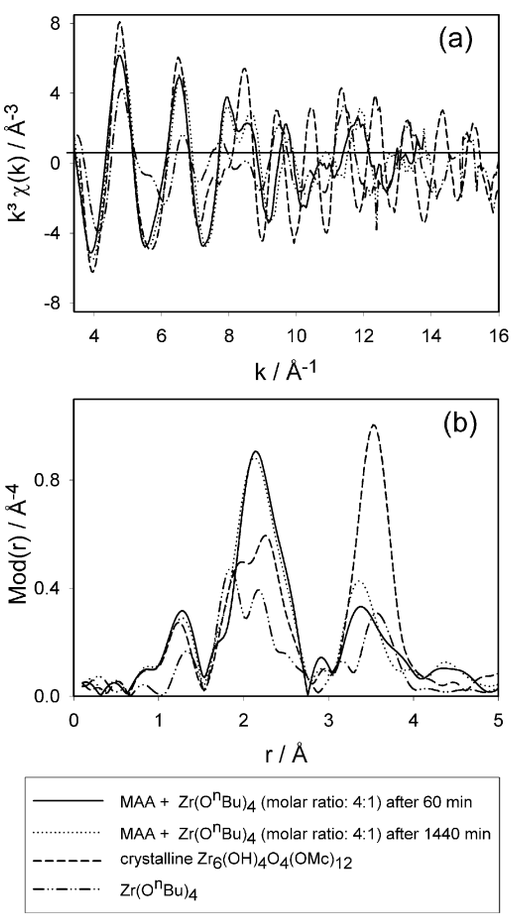

Fig. 2 Experimental $k^3\chi(k)$ functions (a) and their Fourier transforms (b) for a mixture of MAA and 80 wt% $Zr(O^nBu)_4$ in n-butanol (molar ratio: 4:1) from the start of the reaction to 1440 min reaction time at the Zr *K*-edge.

A mixture of 80 wt% $Zr(O^nBu)_4$ in n-butanol solution and 7 molar equivalents of MAA forms the cluster $Zr_4O_2(OMc)_{12}$ [Fig. 1(b)].[7] It is known that the crystalline cluster precipitates much faster compared to $Zr_6(OH)_4O_4(OMc)_{12}$. The faster rate of precipitation of the crystalline compound can also be observed in the absorbance intensity in the X-ray absorption near-edge structure (XANES) spectra of the Zr-*K* edge (Fig. 3). Whereas the 4:1 reaction solution shows nearly no changes in the absorbance during the observation period, the absorbance of the 7:1 solution decreases dramatically. The explanation for this behavior is the fast precipitation of the crystalline cluster from the reaction mixture in the measurement cell, which

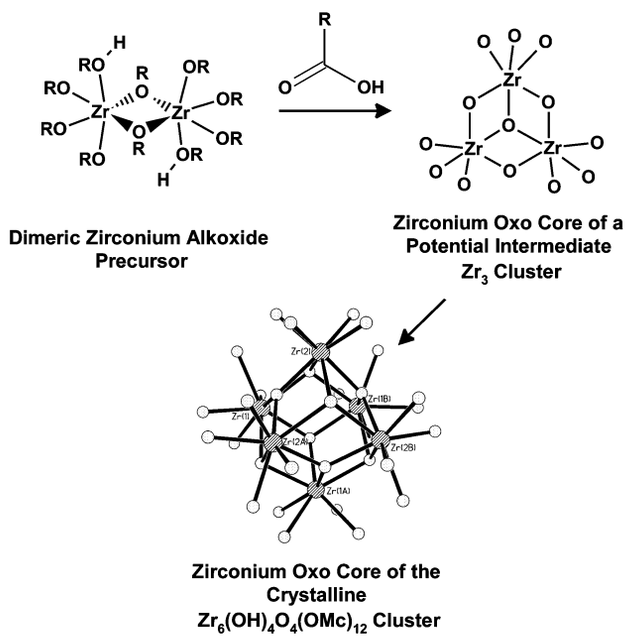

Scheme 2

decreases the Zr content in the solution. After 420 min, the intensity of the absorption is only approximately 1/3 of the original absorbance.

The time evolution of the EXAFS spectra after mixing $Zr(O^nBu)_4$ and 7 equivalents MAA is similar to the observations made in the case of the 4:1 ratio mixture. However, contrary to the 4:1 sample, the oxygen coordination number is around 8 after 30 min and does not change significantly during the reaction (Table 3, Fig. 4). Moreover, in contrast to the crystalline cluster $Zr_6(OH)_4O_4(OMc)_{12}$, the oxygen shells of the EXAFS spectrum of crystalline $Zr_4O_2(OMc)_{12}$ are not well separated and could be fitted with one shell with a mean Zr–O distance of 2.20 Å. The mean oxygen backscatterer peak, however, has two distinct shoulders, while the reaction solution shows again, similar to the 4:1 ratio solution, one average oxygen shell. The number of Zr backscatterers is around 0.6 ± 0.3 initially, and remains low during the reaction (around 0.7 ± 0.1). A possible interpretation is that a mixture of monomeric, dimeric, and higher aggregated Zr species with an average coordination number <1, depending on the composition, is formed in the initial steps of the reaction. The measurement was stopped after 420 min since, due to quantitative crystallization and precipitation of the Zr_4 cluster, no appreciable intensity was detected.

Table 3 Time-dependent structural parameters of a mixture of MAA and 80 wt% $Zr(O^nBu)_4$ in n-butanol (molar ratio: 7:1), determined from the Zr *K*-edge EXAFS spectrum

t/min	A–Bs	r^a/Å	N^b	σ^c/Å	$\Delta E_0{}^d$/eV	*k*-Range/Å^{-1}, fit index
30	Zr–O	2.21 ± 0.02	7.8 ± 0.8	0.095 ± 0.010	18.2	3.12–12.00, 23.9
	Zr–Zr	3.41 ± 0.03	0.6 ± 0.3	0.071 ± 0.017		
60	Zr–O	2.21 ± 0.02	7.7 ± 0.8	0.095 ± 0.010	18.3	3.12–12.00, 23.4
	Zr–Zr	3.40 ± 0.03	0.5 ± 0.3	0.059 ± 0.017		
90	Zr–O	2.21 ± 0.02	8.0 ± 0.8	0.100 ± 0.010	18.3	3.13–12.00, 24.6
	Zr–Zr	3.40 ± 0.03	0.9 ± 0.3	0.081 ± 0.017		
120	Zr–O	2.21 ± 0.02	8.0 ± 0.8	0.097 ± 0.010	18.2	3.11–12.00, 25.8
	Zr–Zr	3.41 ± 0.03	0.9 ± 0.2	0.084 ± 0.017		
180	Zr–O	2.21 ± 0.02	8.1 ± 0.8	0.100 ± 0.010	18.0	3.10–11.60, 25.6
	Zr–Zr	3.42 ± 0.03	0.9 ± 0.2	0.084 ± 0.017		
360	Zr–O	2.22 ± 0.02	7.9 ± 0.8	0.097 ± 0.010	17.8	3.09–11.60, 26.3
	Zr–Zr	3.41 ± 0.03	0.5 ± 0.1	0.055 ± 0.011		
420	Zr–O	2.21 ± 0.02	7.8 ± 0.8	0.095 ± 0.010	18.6	3.10–11.60, 25.8
	Zr–Zr	3.41 ± 0.03	0.7 ± 0.1	0.071 ± 0.014		

[a] Absorber (A)–backscatterer (Bs) distance. [b] Coordination number. [c] Debye–Waller factor, with its calculated deviation. [d] Energy threshold shift.

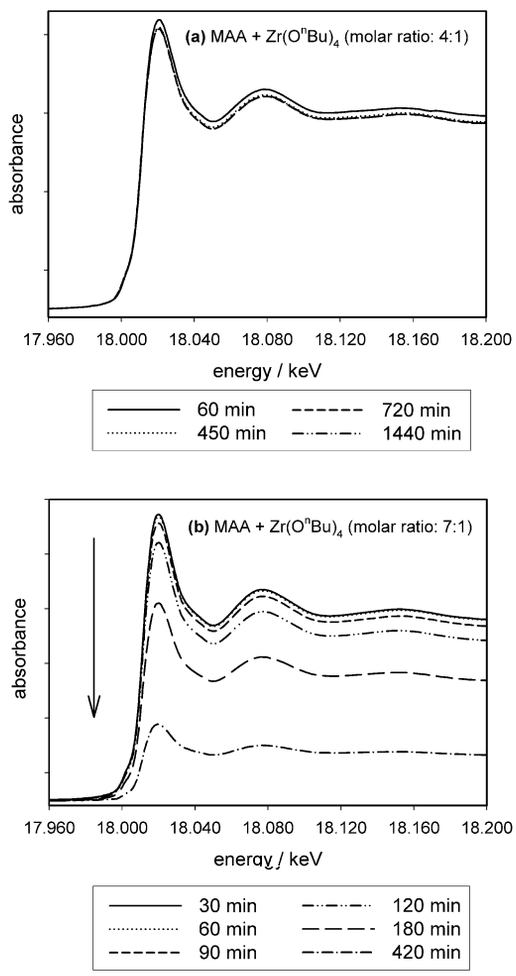

Fig. 3 Comparison of the XANES spectra at the Zr *K*-edge of mixtures of MAA and 80 wt% $Zr(O^nBu)_4$ in n-butanol with molar ratios of (a) 4:1 and (b) 7:1 after various reaction times.

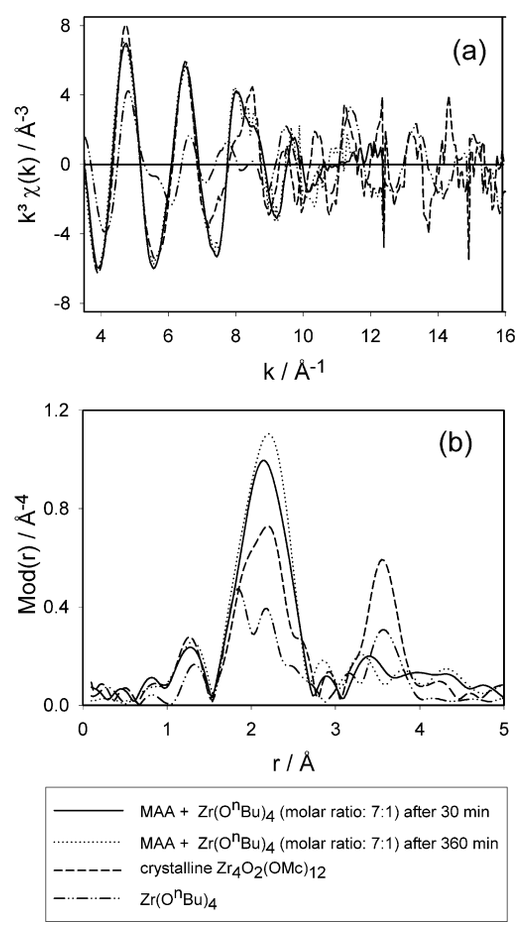

Fig. 4 Experimental $k^3\chi(k)$ functions (a) and their Fourier transforms (b) for a mixture of MAA and 80 wt% $Zr(O^nBu)_4$ in n-butanol (molar ratio: 7:1) from the start of the reaction to 360 min reaction time at the Zr *K*-edge.

NMR results

The reactions in solution of MAA and $Zr(O^nBu)_4$ were followed by 1D and 2D NMR spectroscopy. The proposed development of butyl methacrylate ester (Scheme 1, reaction 2) was of particular interest. A 1:1 mixture of $Zr(O^nBu)_4$ and MAA in C_6D_6 was investigated to prove the formation of ester even at low ratios between the alkoxide and the carboxylic acid. The first spectrum was taken 5 min after MAA was added to $Zr(O^nBu)_4$. After 1 h, a triplet at 4.10 ppm was observed (Fig. 5). This signal was unequivocally assigned to the $-OCH_2-$ protons of butyl methacrylate by applying various 2D NMR methods, such as TOCSY and HMBC. The reaction is fast due to the catalytic activity of the metal alkoxides as Lewis acids in transesterification reactions.[22] On changing the molecular ratio of zirconium alkoxide to MAA, the appearance of the ester signal changes only slightly. However, we noticed a strong dependence of the kinetics of the ester formation on the solvent employed. While ester formation in d^6-benzene is fast, it was even faster in d^2-methylene chloride and much slower in d^8-THF. This behavior can be explained by the different polarity of the solvents. Whereas non-polar

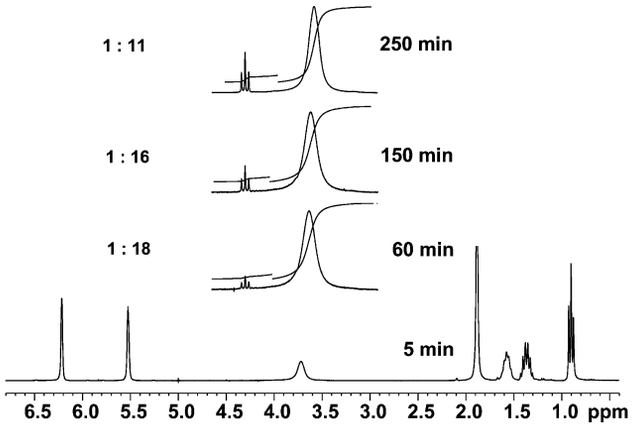

Fig. 5 Time-dependent ^{1}H NMR spectra of a mixture of a 80 wt% $Zr(O^nBu)_4$ in n-butanol and MAA in d^6-benzene, and the integral ratios between the ester and the n-butanol signal.

benzene does not interfere with ester formation, methylene chloride, as a polar solvent, is able to stabilize carboxylate ions formed in the dissociation of the carboxylic acid. These anions react much faster in the substitution of an alkoxide in the zirconium precursor. Hence, the release of alcohol is accelerated and faster esterification reaction can occur. THF, as a potential coordinating solvent, may block coordination sites at the zirconium atom and, hence, slow down the substitution reaction, as well as reduce the catalytic activity of the metal alkoxide.

Raman results

For the Raman measurements, $Zr(O^nPr)_4$ was used as the precursor because the bands arising from this compound could be assigned according to literature values.[23] In the case of the preparation of the investigated zirconium clusters, the structure of the final product is not dependent whether $Zr(O^nBu)_4$ or $Zr(O^nPr)_4$ is used as the zirconium source.[24] The time evolution of the Raman spectrum of the 4:1 molar mixture is presented in Fig. 6. The lower two spectra show the precursors MAA and

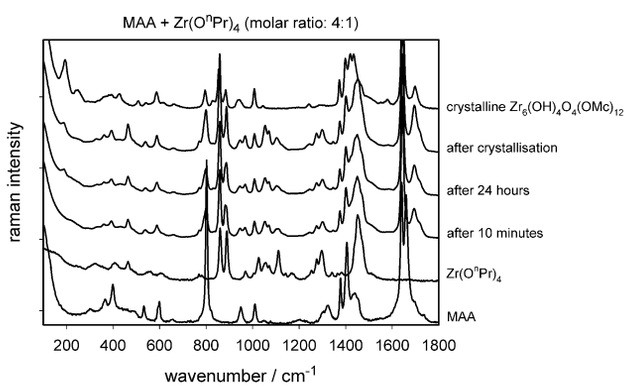

Fig. 6 Comparison of the Raman spectra of a mixture of MAA and 70 wt% $Zr(O^nPr)_4$ in n-propanol (molar ratio: 4:1) at various reaction times. As a reference, the Raman spectrum of the solid product [crystalline $Zr_6(OH)_4O_4(OMc)_{12}$] is also shown.

$Zr(O^nPr)_4$. Pure MAA usually consists of dimers caused by hydrogen bonding. Only 10 min after mixing the two precursors, a distinct band at 1694 cm^{-1} develops, which can be assigned to the MAA monomer. In addition, this band shows a shoulder at about 1720 cm^{-1} that results from the produced ester. This result confirms the fast formation of the ester, which was also observed in the NMR studies. In the other regions of the spectra, a mixture of MAA and $Zr(O^nPr)_4$ bands appear. The spectrum of crystalline $Zr_6(OH)_4O_4(OMc)_{12}$ shows some typical bands in the fingerprint region (Fig. 7). While the peak

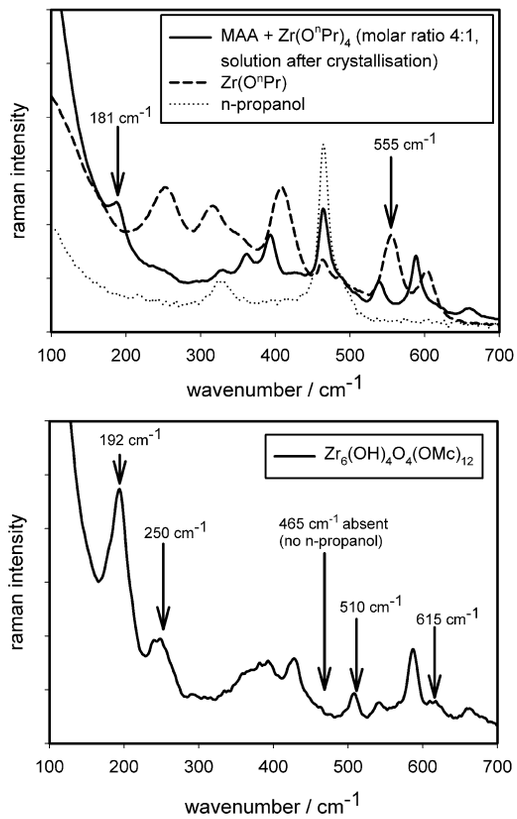

Fig. 7 Comparison of the Raman spectra of a mixture of MAA and 70 wt% $Zr(O^nPr)_4$ in n-propanol (molar ratio: 4:1, after crystallization), n-propanol, and $Zr(O^nPr)_4$ (molar ratio: 4:1) with that of crystalline $Zr_6(OH)_4O_4(OMc)_{12}$.

for the Zr–O^{n}Pr mode at 555 cm^{-1} disappeared completely, additional signals at 192 and 250 cm^{-1}, which most likely can be assigned to Zr–O–Zr modes, appeared. This is consistent with the molecular structure of the crystalline product which exclusively contains coordinated methacrylate and no alkoxide ligands at the Zr atom. In the crystalline product, MAA bands, which are due to the inclusion of MAA in the voids of the crystal lattice,[7] were still observed at 1694 and 802 cm^{-1}. The cluster $Zr_4O_2(OMc)_{12}$, formed from a 7:1 ratio does not contain methacrylic acid in the crystalline lattice and, therefore, its specific bands cannot be observed.

HPLC results

HPLC was applied as an additional method to investigate ester formation in the solution and the effect of the Zr alkoxide on it. First, a mixture of four MAA esters with different chain lengths (methyl, ethyl, propyl, and butyl) in acetonitrile were investigated by HPLC as reference samples [Fig. 8(a), dotted line]. Four signals were detected at t = 3.83 [identified as methyl methacrylate (MMA)], 4.83 [identified as ethyl methacrylate (EMA)], 6.21 [identified as propyl methacrylate (PMA)], and at 8.06 min [identified as butyl methacrylate (BMA)]. In addition, the retention time of MAA in acetonitrile was measured as a further reference, and the signal was observed at 1.86 min. In the MAA + $Zr(O^nPr)_4$ mixture after 10 min reaction, two signals in the HPLC chromatogram were observed at 1.86 (4:1) and 6.26 min (7:1) [Fig. 8(a) solid line]. These signals were assigned to MAA and PMA. This result shows that the formation of the ester in the presence of $Zr(O^nPr)_4$ is very fast. Furthermore, since no signal at ~6.2 min, typical for PMA, was found in the chromatogram of a mixture of MAA + n-propanol after 10, 30, and 120 min reaction time, it can be concluded that the Zr alkoxide catalyzes the esterification.

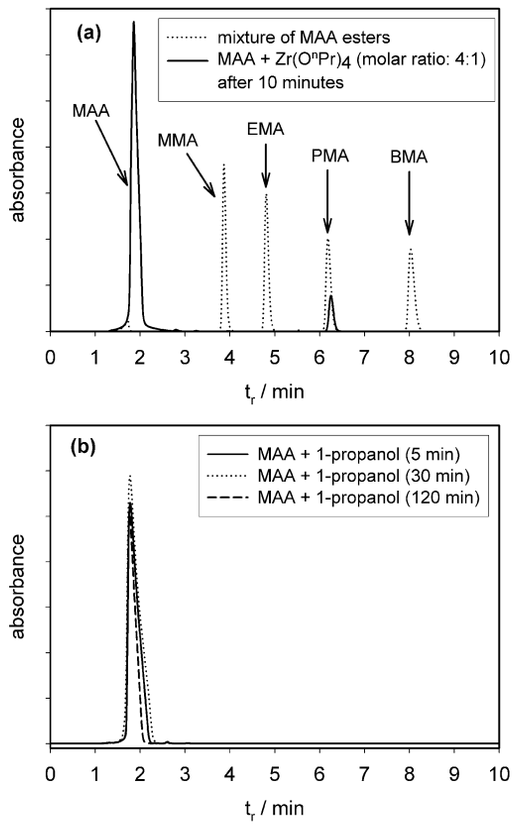

Fig. 8 HPLC chromatograms of (a) mixtures of methyl methacrylate (MMA), ethyl methacrylate (EMA), n-propyl methacrylate (PMA), and n-butyl methacrylate (BMA), and of MAA and 70 wt% $Zr(O^nPr)_4$ in n-propanol (molar ratio: 4:1) after 10 min reaction time, and (b) a mixture of MAA and n-propanol (molar ratio 1:1) after various reaction times.

Thus, the HPLC studies supports the results obtained from NMR and Raman.

Summary

In summary, a combination of complementary methods was used to investigate the reactions between zirconium alkoxides and methyl methacrylate. The time-dependent measurements confirm the postulated reaction mechanism for the formation of metal oxo clusters in solutions. Results obtained from the EXAFS measurements show that the precursor alkoxide reacts fast and forms species in which the alkoxide dimers are degraded and the structure of the final cluster is pre-formed. NMR and HPLC measurements reveal that ester formation in the solution is fast due to catalysis of the esterification by the zirconium alkoxide. Raman investigations verified both the fast ester formation and the fast reaction of the metal alkoxide precursor with the carboxylic acid.

Experimental

All chemicals were obtained from Aldrich and used without further purification. All reactions were carried out under an argon atmosphere. Cluster formation reactions were carried out according to literature procedures.[7]

EXAFS measurements and analysis

The EXAFS measurements of the samples were performed on beamline X1.1 (RÖMO II) at the Hamburger Synchrotronstrahlungslabor (HASYLAB) at DESY (Hamburg, Germany) under ambient conditions. The synchrotron beam current was between 80–140 mA (positron energy 4.45 GeV). For the measurements at the zirconium *K*-edge (17998.0 eV), an Si(311) double-crystal monochromator was used. The tilt of the second monochromator crystal was set to 30% harmonic rejection. Energy calibration was performed with the corresponding metal foil. Energy resolution was estimated to be 5 eV for the Zr *K*-edge. All experiments were carried out in transmission mode with argon-filled ion chambers at 25 °C. For the measurements in the solid state, the samples were embedded under an inert gas atmosphere in a polyethylene matrix and pressed into pellets. The liquid samples for the EXAFS studies were also prepared under an inert gas atmosphere and filled into a specially designed transmission sample cell for liquids. The concentration of all samples was adjusted to yield an absorption jump of $\Delta\mu d \approx 1.5$. Data evaluation started with background absorption removal from the experimental absorption spectrum by subtraction of a Victoreen-type polynomial. Then the background-subtracted spectrum was convoluted with a series of increasingly broader Gaussian functions and the common intersection point of the convoluted spectra was taken as energy E_0.[25,26] To determine the smooth part of the spectrum, corrected for pre-edge absorption, a piecewise polynomial was used. It was adjusted in such manner that the low-*R* components of the resulting Fourier transformation were minimal. After division of the background-subtracted spectrum by its smooth part, the photon energy was converted to photoelectron wave numbers *k*. The resulting EXAFS function was weighted with k^3. Data analysis in *k* space was performed according to the curved wave multiple scattering formalism of the program EXCURV92 with XALPHA phase and amplitude functions.[27] The mean free path of the scattered electrons was calculated from the imaginary part of the potential (VPI was set to −4.00) and an overall energy shift (ΔE_0) was assumed. The amplitude reduction factor (AFAC) was set to a value of 0.8. In the case of the EXAFS analysis of the pure clusters, the coordination numbers were fixed according to the crystallographically determined values; in the case of $Zr(O^nBu)_4$, the coordination numbers were fixed according to the model of Peter *et al.*[14]

Raman measurements

The Raman spectra were recorded with a Bruker RFS 100/S Fourier transform (FT) Raman spectrometer using an air-cooled near infrared Nd:YAG laser with a wavelength of 1064 nm. For the solid samples, a few mg of the materials were placed into a sample holder for solids and irradiated with laser light (laser power 150 mW). The scattered light was collected with a high-sensitivity Ge diode (cooled with liquid nitrogen). 400 scans were accumulated (spectral resolution 2 cm^{-1}) for an average measurement. The measurements of liquid samples were performed in a quartz sample cell (laser power 500 mW).

NMR measurements

The NMR spectra were recorded on a Bruker Avance 300 spectrometer (300.13 {^{1}H} and 75.47 MHz {^{13}C}), equipped with a 5 mm broadband head and a *z*-gradient unit. 1D and 2D spectra were measured with Bruker standard pulse sequences: HSQC (heteronuclear single quantum correlation), HMBC (heteronuclear multiple bond correlation), COSY (correlated spectroscopy), TOCSY (total correlation spectroscopy).

HPLC measurements

The HPLC measurements were performed on a HP 1100 Series HPLC system equipped with an LiChrosorb column (RP-18, 6 μm) from Merck and a UV/Vis detector. An acetonitrile–water mixture was used as eluent and the UV absorption at 254 nm was measured for detection. The sample was prepared as follows: MAA and 70 wt.% $Zr(O^nPr)_4$ in n-propanol were mixed in a molar ratio of 4:1. After 10 min reaction time, 1 ml

H_2O + 1 ml acetonitrile were added to the solution. The solution was filtered and 10 μL of the filtrate were injected onto the HPLC column. Samples of methyl methacrylate (MMA), ethyl methacrylate (EMA), n-propyl methacrylate (PMA), n-butyl methacrylate (BMA), all diluted in acetonitrile, a mixture of all four esters in acetonitrile, and a mixture of MAA and n-propanol (molar ratio: 1:1; after 10, 30, and 120 min reaction time) in acetonitrile were measured as references.

Acknowledgements

We wish to thank HASYLAB at DESY, Hamburg for kind support of the synchrotron experiments at beamline X1.1 (RÖMO II) and the Fonds zur Förderung der Wissenschaftlichen Forschung (FWF), Austria, for their financial support of this project. In addition, we also thank Stefan Jagiella for technical assistance.

References

1 P. Judeinstein and C. Sanchez, *J. Mater. Chem.*, 1996, **6**, 511.
2 A. D. Pomogailo, *Russ. Chem. Rev.*, 2000, **69**, 53.
3 U. Schubert, *Chem. Mater.*, 2001, **13**, 3487.
4 G. Kickelbick, *Prog. Polym. Sci.*, 2002, in press.
5 S. Doeuff, Y. Dromzee, F. Taulelle and C. Sanchez, *Inorg. Chem.*, 1989, **28**, 4439.
6 U. Schubert, E. Arpac, W. Glaubitt, A. Helmerich and C. Chau, *Chem. Mater.*, 1992, **4**, 291.
7 G. Kickelbick and U. Schubert, *Chem. Ber.*, 1997, **130**, 473.
8 G. Kickelbick and U. Schubert, *Eur. J. Inorg. Chem.*, 1998, 159.
9 G. Kickelbick, P. Wiede and U. Schubert, *Inorg. Chim. Acta*, 1999, **284**, 1.
10 G. Kickelbick and U. Schubert, *J. Chem. Soc., Dalton Trans.*, 1999, 1301.
11 G. Kickelbick and U. Schubert, *Monatsh. Chem.*, 2001, **132**, 13.
12 H. Bertagnolli and T. S. Ertel, *Angew. Chem., Int. Ed. Engl.*, 1994, **1994**, 45.
13 G. Kickelbick, M. P. Feth, H. Bertagnolli, B. Moraru, G. Trimmel and U. Schubert, *Monatsh. Chem.*, 2002, **133**, 919.
14 D. Peter, T. S. Ertel and H. Bertagnolli, *J. Sol-Gel Sci. Technol.*, 1995, **5**, 5.
15 B. A. Vaartstra, J. C. Huffman, P. S. Gradeff, L. G. Hubert-Pfalzgraf, J.-C. Daran, S. Parraud, K. Yunlu and K. G. Caulton, *Inorg. Chem.*, 1990, **29**, 3126.
16 W. J. Evans, M. A. Ansari and J. W. Ziller, *Inorg. Chem.*, 1999, **38**, 1160.
17 T. J. Boyle, J. J. Gallegos III, D. M. Pedrotty, E. R. Mechenbier and B. L. Scott, *J. Coord. Chem.*, 1999, **47**, 155.
18 W. J. Evans, M. A. Ansari and J. W. Ziller, *Polyhedron*, 1998, **17**, 869.
19 Z. A. Starikova, E. P. Turevskaya, N. I. Kozlova, N. Y. Turova, D. V. Berdyev and A. I. Yanovsky, *Polyhedron*, 1999, **18**, 941.
20 P. S. Ammala, J. D. Cashion, C. M. Kepert, K. S. Murray, B. Moubaraki, L. Spiccia and B. O. West, *J. Chem. Soc., Dalton Trans.*, 2001, 2032.
21 M. A. Walters, K.-C. Lam, S. Damo, R. D. Sommer and A. L. Rheingold, *Inorg. Chem. Commun.*, 2000, **3**, 316.
22 M. D. Curran, T. E. Gedris and A. E. Stiegman, *Chem. Mater.*, 1998, **10**, 1604.
23 J. Chaibi, M. Henry, H. Zarrouk, N. Gharbi and J. Livage, *J. Non-Cryst. Solids*, 1994, **170**, 1.
24 G. Kickelbick and U. Schubert, unpublished results.
25 T. S. Ertel, H. Bertagnolli, S. Hückmann, U. Kolb and D. Peter, *Appl. Spectrosc.*, 1992, **46**, 690.
26 M. Newville, P. Livins, Y. Yakoby, J. J. Rehr and E. A. Stern, *Phys. Rev. B*, 1993, **47**, 14126.
27 S. J. Gurman, N. Binsted and I. Ross, *J. Phys. C*, 1986, **19**, 1845.